Monthly Notices
of the
ROYAL ASTRONOMICAL SOCIETY

Mon. Not. R. Astron. Soc. **426,** 1361–1368 (2012) doi:10.1111/j.1365-2966.2012.21805.x

The effect of the linear term on the wavelet estimator of primordial non-Gaussianity

A. Curto,⋆ E. Martínez-González and R. B. Barreiro

Instituto de Física de Cantabria, CSIC-Universidad de Cantabria, Avda. de los Castros s/n, 39005 Santander, Spain

Accepted 2012 July 25. Received 2012 July 25; in original form 2012 April 25

ABSTRACT

In this work, we present constraints on different shapes of primordial non-Gaussianity using the *Wilkinson Microwave Anisotropy Probe* (*WMAP*) seven-year data and the spherical Mexican hat wavelet $f_{\rm nl}$ estimator including the linear term correction. In particular, we focus on the local, equilateral and orthogonal shapes. We first analyse the main statistical properties of the wavelet estimator and show the conditions to reach optimality. We include the linear term correction in our estimators and compare the estimates with the values already published using only the cubic term. The estimators are tested with realistic *WMAP* simulations with anisotropic noise and the *WMAP* KQ75 sky cut. The inclusion of the linear term correction shows a negligible improvement ($\leq$1 per cent) in the error bar for any of the shapes considered. The results of this analysis show that, in the particular case of the wavelet estimator, the optimality for *WMAP* anisotropy levels is basically achieved with the mean subtraction, and in practical terms there is no need of including a linear term once the mean has been subtracted. Our best estimates are now $\hat{f}_{\rm nl}^{\rm (loc)} = 39.0 \pm 21.4$, $\hat{f}_{\rm nl}^{\rm (eq)} = -62.8 \pm 154.0$ and $\hat{f}_{\rm nl}^{\rm (ort)} = -159.8 \pm 115.1$. We have also computed the expected linear term correction for simulated *Planck* maps with anisotropic noise at 143 GHz following the *Planck* Sky Model and including a mask. The improvement achieved in this case for the local $f_{\rm nl}$ error bar is also negligible (0.4 per cent).

Key words: methods: data analysis – cosmic background radiation – cosmology: observations.

1 INTRODUCTION

In the recent years, the spherical Mexican hat wavelet (SMHW; Martínez-González et al. 2002) has been used to construct a new type of estimator for the primordial non-Gaussianity in the cosmic microwave background (CMB) characterized by the non-linear coupling parameter $f_{\rm nl}$ (Curto et al. 2009a, 2011b; Curto, Martínez-González & Barreiro 2009b, 2010, 2011a). One of the particularities of the wavelet estimator as it has been traditionally presented in the literature compared with direct bispectrum-based estimators (Komatsu & Spergel 2001; Komatsu et al. 2002, 2003, 2005, 2009, 2011; Babich, Creminelli & Zaldarriaga 2004; Babich 2005; Creminelli et al. 2006; Creminelli, Senatore & Zaldarriaga 2007; Spergel et al. 2007; Yadav & Wandelt 2008; Elsner & Wandelt 2009; Smith, Senatore & Zaldarriaga 2009; Liguori et al. 2010; Senatore, Smith & Zaldarriaga 2010; Smidt et al. 2010; Fergusson, Liguori & Shellard 2010a,b; Fergusson & Shellard 2011) is the absence of a linear term. In the bispectrum-based estimators, the linear term plays a key role to achieve optimality in the cases where the rotational invariance of the CMB is broken because of different instrumental complexities such as anisotropic noise or partial sky coverage (see for example Creminelli et al. 2006, 2007; Yadav & Wandelt 2010; Fergusson & Shellard 2011).

The computational difficulties related to the inversion of the covariance matrix present in the bispectrum estimator, especially in future data sets with higher $\ell_{\rm max}$ as for example *Planck*,[1] together with the unknown effect that different systematics from the instrument and background residuals might have on the estimates, motivated the search for new estimators based on different tools such as the SMHW described in this paper, the binned bispectrum (Bucher, van Tent & Carvalho 2010), the general modal expansion and polyspectra estimation (Fergusson et al. 2010b; Fergusson & Shellard 2011), the needlets (Marinucci et al. 2008; Pietrobon et al. 2009; Rudjord et al. 2009; Donzelli et al. 2012), the HEALPIX wavelet (Casaponsa et al. 2011a), neural networks (Casaponsa et al. 2011b) or a Bayesian approach (Elsner & Wandelt 2010; Elsner, Wandelt & Schneider 2010) among others.

In a previous paper (Curto et al. 2011a), we described the main features of the wavelet estimator based on the cubic statistics constructed from the SMHW coefficient maps. Those cubic terms were written as a function of the non-linear coupling parameter $f_{\rm nl}$ and the bispectrum of the primordial non-Gaussianity. In that paper,

⋆E-mail: curto@ifca.unican.es

[1] http://www.esa.int/planck

we also showed that the power of the method to detect $f_{\rm nl}$, that is the variance of this parameter $\sigma^2(f_{\rm nl})$, matches that of the direct bispectrum-based estimators for ideal conditions (full sky and isotropic noise) and realistic conditions (partial sky coverage and anisotropic noise). The wavelet estimator variance was obtained in two different ways: through the Fisher matrix and by means of Monte Carlo (MC) simulations, providing very similar results. A remarkable result of these works is the fact that the wavelet estimator is, in practice, able to reach optimality on the $f_{\rm nl}$ estimation without including any linear term correction. However, from several works (see for example Creminelli et al. 2006; Fergusson & Shellard 2011) it has been shown that in order to reach minimum variance, all the cubic estimators need a linear term correction. A recent work has solved this apparent controversy (Donzelli et al. 2012) by showing that in *Wilkinson Microwave Anisotropy Probe* (*WMAP*)[2] anisotropy conditions, the linear term correction is nearly equivalent to the mean subtraction performed for each wavelet coefficient map in the wavelet estimator.

In this paper, we re-examine the main statistical properties of the wavelet estimator and show the conditions to reach optimality. We compute the linear term correction for the local, equilateral and orthogonal $f_{\rm nl}$ shapes. In particular, we see that the linear term correction for the local case provides a 1 per cent reduction in the error bars (in agreement with Donzelli et al. 2012, for the SMHW), while the correction for the other shapes is even smaller. Section 2 introduces the SMHW estimator, its variance and its linear correction. In Section 3, the estimator with its linear correction is applied to *WMAP* seven-year data for the local, equilateral and orthogonal shape. In Section 4, we explore the linear correction on *Planck* simulations at 143 GHz for the local shape, and in Section 5, the conclusions are presented.

2 THE WAVELET APPROACH

In this section, we present an approach for the $f_{\rm nl}$ estimator based on the statistical properties of the cubic terms of the SMHW coefficients averaged over the sky. In this case, we exploit the property of the SMHW wavelet that performs a strong decorrelation of the data at distances larger than the wavelet resolution. The expected values of the cubic terms in the sky are obtained from the sum of a large number of almost independent elements, and therefore, its distribution will be close to Gaussian by the central limit theorem. We will first review the SMHW and its decorrelation properties, and then, we will construct the wavelet estimator based on those properties including the linear term correction.

2.1 The SMHW coefficients and their correlation

Detailed information about the SMHW and a (non-complete) list of applications to the CMB maps and cosmology can be found in Antoine & Vandergheynst (1998), Martínez-González et al. (2002), Cayón et al. (2003), Vielva, Martínez-González & Tucci (2006), Vielva (2007), McEwen et al. (2007), Martínez-González (2008), Zhang et al. (2011) and Yu et al. (2012).

Given a function $f(\boldsymbol{n})$ defined at a position $\boldsymbol{n}$ on the sphere and a continuous wavelet family on that space $\Psi(\boldsymbol{n};\boldsymbol{b}, R)$, we define the continuous wavelet transform as

$$w(R;\boldsymbol{b}) = \int {\rm d}\boldsymbol{n}\, f(\boldsymbol{n})\Psi(\boldsymbol{n};\boldsymbol{b}, R), \tag{1}$$

[2] http://map.gsfc.nasa.gov/

where $\boldsymbol{b}$ is the position on the sky at which the wavelet coefficient is evaluated, R is the scale of the wavelet and $\boldsymbol{\Psi}_S(\theta; R) \equiv \Psi(\boldsymbol{n}(\theta,\phi);\boldsymbol{0}, R)$ is given by

$$\boldsymbol{\Psi}_S(\theta; R) = \frac{1}{\sqrt{2\pi}N(R)}\left[1+\left(\frac{y}{2}\right)^2\right]^2\left[2-\left(\frac{y}{R}\right)^2\right]{\rm e}^{-y^2/(2R^2)}, \tag{2}$$

where

$$N(R) = R\left(1+\frac{R^2}{2}+\frac{R^4}{4}\right)^{1/2} \tag{3}$$

and

$$y = 2\tan\left(\frac{\theta}{2}\right). \tag{4}$$

Considering a set of different angular scales $\{R_i\}$, we define a third-order statistic depending on three scales $\{i, j, k\}$ (Curto et al. 2009b)

$$q_{ijk} = \frac{1}{4\pi}\frac{1}{\sigma_i\sigma_j\sigma_k}\int {\rm d}\boldsymbol{n}\, w(R_i,\boldsymbol{n})w(R_j,\boldsymbol{n})w(R_k,\boldsymbol{n}), \tag{5}$$

where σ_i is the dispersion of the wavelet coefficient map $w(R_i,\boldsymbol{n})$. In the particular case of $R_0 = 0$, $w(R_0,\boldsymbol{n}) \equiv f(\boldsymbol{n})$. For a particular pixelization on the sphere, equation (5) can be written as

$$q_{ijk} = \frac{1}{N_{ijk}}\sum_{p=0}^{N_{\rm pix}-1}\frac{w_i(p)w_j(p)w_k(p)}{\sigma_i\sigma_j\sigma_k}, \tag{6}$$

where $N_{\rm pix}$ is the total number of pixels of the map, N_{ijk} is the number of pixels available after combining the extended masks corresponding to the three scales R_i, R_j and R_k and $w_i(p) \equiv w(R_i, p) - \langle w(R_i)\rangle$ is the wavelet coefficient in the pixel p evaluated at the scale R_i after subtracting the mean value over the wavelet coefficient map outside its extended mask.

Using the properties of the wavelet, we may write the wavelet transform of the temperature map in the next form (Curto et al. 2011a)

$$w(R_i,\boldsymbol{n}) = \sum_{\ell m} a_{\ell m}\omega_\ell(R_i)Y_{\ell m}(\boldsymbol{n}). \tag{7}$$

Using the isotropic properties of the CMB and the properties of the wavelet, we can obtain the angular coefficient correlation $C_{ij}(\theta)$ between any pair of pixels $\boldsymbol{n}$ and $\boldsymbol{n}'$ separated by an angular distance $\boldsymbol{n}\boldsymbol{n}' = \cos(\theta)$ and for two angular scales R_i and R_j:

$$\begin{aligned} C_{ij}(\theta) &\equiv \langle w(R_i,\boldsymbol{n})w(R_j,\boldsymbol{n})\rangle \\ &= \sum_\ell \frac{2\ell+1}{4\pi}C_\ell\omega_\ell(R_i)\omega_\ell(R_j)P_\ell\left(\cos(\theta)\right), \end{aligned} \tag{8}$$

where $\omega_\ell(R)$ is the window function of the wavelet at a scale R and it is given by the harmonic transform of the mother wavelet of the SMHW (Martínez-González et al. 2002; Sanz et al. 2006). The dispersion of the wavelet coefficients at scale R_i is simply given by $\sigma_i = C_{ii}(\theta = 0)^{1/2}$.

In Fig. 1, we show the correlation of the wavelet coefficients as a function of the angular distance θ for several values of the resolution scale R. As can be seen, the SMHW produces an effective decorrelation of the signal at angular distances above the resolution scale R.

2.2 The wavelet estimator

Considering the strong decorrelation produced by the convolution of the SMHW on the temperature anisotropies, we can now apply the

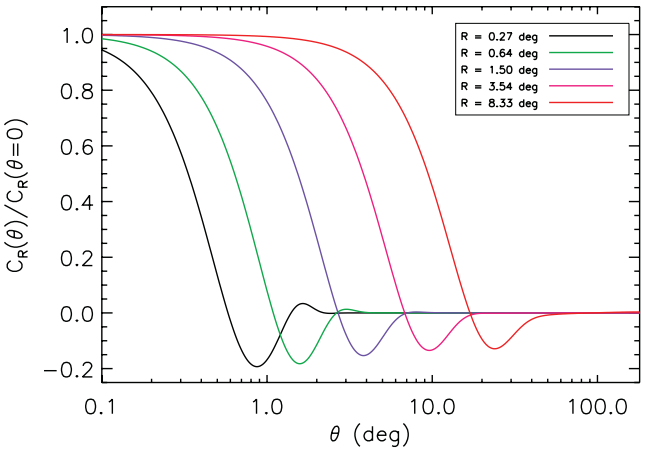

Figure 1. The normalized correlation functions for different wavelet coefficient maps are plotted. From left to right, the curves correspond to maps convolved with an SMHW of scale $R = 0.^{\circ}27$, $0.^{\circ}64$, $1.^{\circ}50$, $3.^{\circ}54$ and $8.^{\circ}33$, respectively.

central limit theorem to the cubic statistics defined in equation (5). Since the average value is calculated from the sum of a very large number of almost independent elements (of the order of the number of pixels in the sphere with size that of the resolution scale R), then its distribution should be very close to a Gaussian. This is actually seen in Fig. 2, where the distribution of the cubic terms for different SMHW scales is shown. These distributions have been obtained from MC simulations of Gaussian temperature anisotropies.

The previous results indicate that, for Gaussian temperature anisotropies, a good representation of the n-point distribution of the quantities q_{ijk} can be given in terms of a multinormal distribution. Allowing now for the presence of weak non-Gaussianity for the temperature anisotropies (e.g. an amplitude for the primordial non-Gaussianity consistent with *WMAP* data), one can use the next likelihood for the $f_{\rm nl}$ parameter:

$$L(f_{\rm nl}) \propto {\rm e}^{-\chi^2(f_{\rm nl})/2}, \tag{9}$$

where $\chi^2(f_{\rm nl})$ is given by

$$\chi^2(f_{\rm nl}) = \sum_{ijk,rst} \left(q_{ijk}^{\rm obs} - f_{\rm nl}\alpha_{ijk}\right) \mathbf{C}^{-1}_{ijk,rst} \left(q_{rst}^{\rm obs} - f_{\rm nl}\alpha_{rst}\right), \tag{10}$$

where $q_{ijk}^{\rm obs}$ are the cubic statistics corresponding to the observed data, $\alpha_{ijk} = \langle q_{ijk}\rangle_{f_{\rm nl}=1}$ and $\mathbf{C}_{ijk,rst}$ is the covariance matrix of the cubic statistics. A further test to check that the q_{ijk} are normally distributed can be done by considering the property that $\Delta\chi^2(f_{\rm nl}) = \chi^2(f_{\rm nl}) - \chi^2_{\rm min}(f_{\rm nl})$ is a χ^2 distribution with one degree of freedom. In particular, $\Delta\chi^2(f_{\rm nl}) = 1$ (4) should provide the 1 (2)σ or 68 per cent (95 per cent) confidence intervals for the $f_{\rm nl}$ parameter. Using MC simulations, we have checked that this is the case for the q_{ijk} statistics.

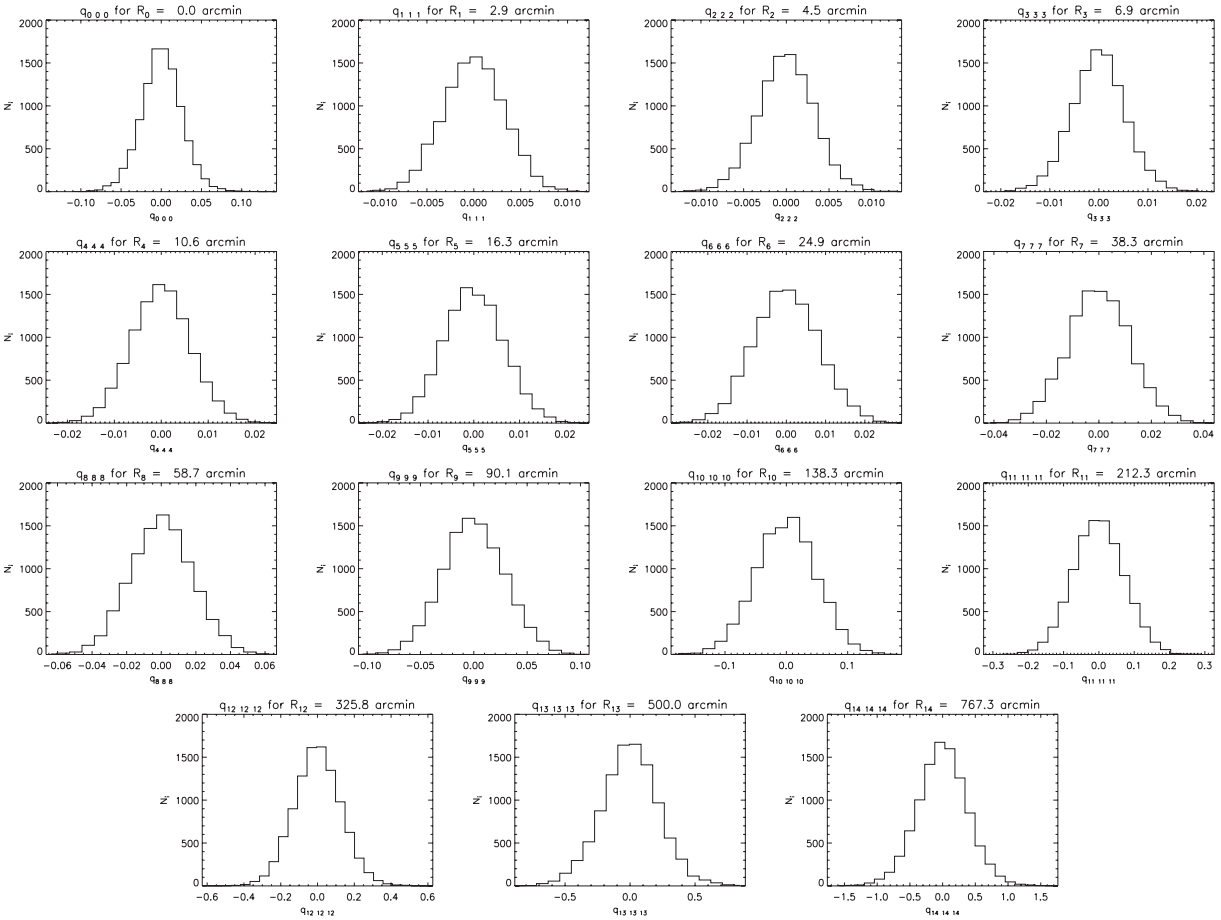

Figure 2. Histograms of the cubic statistics q_{iii} for the different angular scales R_i considered in previous works (Curto et al. 2011a,b).

After straightforward calculation, it can be easily seen that the $f_{\rm nl}$ estimator in this case is given by

$$\hat{f}_{\rm nl} = \frac{\sum \alpha_{ijk} \mathbf{C}^{-1}_{ijk,rst} q_{rst}}{\sum \alpha_{ijk} \mathbf{C}^{-1}_{ijk,rst} \alpha_{rst}}, \tag{11}$$

while that the variance of the $\hat{f}_{\rm nl}$ parameter in equation (11) is given by

$$\sigma^2_{\rm F}(\hat{f}_{\rm nl}) = \frac{-1}{\left\{ \frac{\partial^2 \log L(f_{\rm nl})}{\partial f^2_{\rm nl}} \right\}_{f_{\rm nl}=\hat{f}_{\rm nl}}} = \frac{1}{\frac{1}{2}\left\{ \frac{\partial^2 \chi^2(f_{\rm nl})}{\partial f^2_{\rm nl}} \right\}_{f_{\rm nl}=\hat{f}_{\rm nl}}} = \frac{1}{\sum_{ijk,rst} \alpha_{ijk} \mathbf{C}^{-1}_{ijk,rst} \alpha_{rst}}. \tag{12}$$

This estimator has already been shown to be nearly optimal on *WMAP* data (Curto et al. 2009a,b, 2010, 2011a,b) without the need of subtracting any linear term. However, as stated in Donzelli et al. (2012), from all the possible cubic combinations of three Gaussian variables, the Wick polynomials are shown to have minimum variance. This implies that in order to have a strictly speaking minimum variance estimator, a linear term correction needs to be included. In fact the linear term subtraction is equivalent to the mean subtraction at each wavelet coefficient map (Donzelli et al. 2012) for low levels of anisotropy. This is indeed the procedure that has been followed in Curto et al. (2009a,b, 2010, 2011a,b), and it explains the competitive results obtained just by subtracting the mean using the estimator in equation (11).

The linear term correction for the wavelet estimator can be written as

$$\hat{f}^{\rm (total)}_{\rm nl} = \hat{f}^{\rm (cubic)}_{\rm nl} - \hat{f}^{\rm (linear)}_{\rm nl}, \tag{13}$$

where $\hat{f}^{\rm (cubic)}_{\rm nl}$ is given by equation (11) and

$$\hat{f}^{\rm (linear)}_{\rm nl} = \sigma^2_{\rm F}(\hat{f}_{\rm nl}) \sum_{ijk,rst} \alpha_{ijk} \mathbf{C}^{-1}_{ijk,rst} q^{(L)}_{rst} \tag{14}$$

with

$$q^{(L)}_{ijk} = \frac{1}{N_{ijk}} \sum_p \left\{ \left\langle \frac{w_i(p)}{\sigma_i} \frac{w_j(p)}{\sigma_j} \right\rangle \frac{w_k(p)}{\sigma_k} + \left\langle \frac{w_i(p)}{\sigma_i} \frac{w_k(p)}{\sigma_k} \right\rangle \frac{w_j(p)}{\sigma_j} + \left\langle \frac{w_j(p)}{\sigma_j} \frac{w_k(p)}{\sigma_k} \right\rangle \frac{w_i(p)}{\sigma_i} \right\}. \tag{15}$$

In the next sections, we apply the wavelet estimator to *WMAP* seven-year data as well as to *Planck* simulations and compare the results obtained with and without the linear term correction.

3 APPLICATION TO *WMAP* V+W DATA

We have computed the linear term correction to the cubic wavelet $f_{\rm nl}$ estimator for the three shapes with a relevant interest in many inflationary models: the local, equilateral and orthogonal shapes (see for example Bartolo et al. 2004; Senatore et al. 2010; Komatsu et al. 2011). The estimator can be easily applied to other bispectra with a separable shape (Curto et al. 2011a). Results taking into account only the cubic contribution are already published (Curto et al. 2011b).

We have selected the same set of 15 angular scales from $R_0 = 0$ to $R_{14} = 767.3$ arcmin as used in Curto et al. (2011b). We have considered the V+W *WMAP* data optimally weighted by the $N_{\rm hits}$ maps per radiometer in order to maximize the signal-to-noise ratio. We also consider the same *WMAP* KQ75 mask and its extended masks for each wavelet angular scale. The cubic covariance matrix has been computed using 10 000 Gaussian simulations. A principal component analysis has been performed in order to avoid contamination from the lowest noisy eigenvalues of this covariance matrix without losing non-Gaussian signal (Curto et al. 2011a). The two-point correlation matrices needed for the linear term correction have also been estimated with 64 000 Gaussian simulations. This number of simulations is needed in order to achieve the required precision in the estimation of the correlation matrices.

We have applied the estimator to one set of 10 000 Gaussian maps and the *WMAP* data. The results are presented in Fig. 3 for the three considered shapes. In the left-hand panels, the red histograms correspond to the best-fitting $f_{\rm nl}$ values obtained with the cubic estimator and the black histograms correspond to the best-fitting $f_{\rm nl}$ values after the linear term correction. The vertical lines correspond to the actual *WMAP* data values estimated with the cubic estimator (red) and the linearly corrected estimator (black). In the right-hand panels, we compare the best-fitting $f_{\rm nl}$ values for the same set of Gaussian simulations. Note that both $f^{\rm (cubic)}_{\rm nl}$ and $f^{\rm (total)}_{\rm nl}$ are highly correlated and the deviations are not significant. Finally, in Tables 1–3 the previous results are summarized. We present the *WMAP* seven-year $f_{\rm nl}$ best-fitting values for the cubic estimator $f^{\rm (cubic)}_{\rm nl}$, the linear estimator $f^{\rm (linear)}_{\rm nl}$ and $f^{\rm (total)}_{\rm nl}$ for the clean and raw (uncleaned) maps. The Fisher $f_{\rm nl}$ error bar as described in equation 25 of Curto et al. (2011a) is also provided. For each case, we observe a small reduction of the error bars when the linear term is included. The largest correction is introduced in the local shape, where σ is reduced from $\sigma(f_{\rm nl}) = 21.6$ to 21.4 (i.e. a reduction of 1 per cent, in agreement with Donzelli et al. 2012). The correction for the other two cases, equilateral and orthogonal, is also negligible (about 0.2 and 0.1 per cent, respectively). This is in agreement with Creminelli et al. (2006) for the equilateral shape, where the standard deviations of $f_{\rm nl}$ without the linear term were found closer to the lower Fisher limit than in the local shape, suggesting a less important contribution of the linear term correction.

Our best-fitting values, computing $\sigma(f_{\rm nl})$ with 10 000 Gaussian simulations to characterize the errors, are presented below for the three shapes.

Local form results:[3]

(i) $f^{\rm (cubic)}_{\rm nl} = 38.9 \pm 21.6$
(ii) $f^{\rm (total)}_{\rm nl} = 39.0 \pm 21.4$

Equilateral form results:

(i) $f^{\rm (cubic)}_{\rm nl} = -53.3 \pm 154.3$
(ii) $f^{\rm (total)}_{\rm nl} = -62.8 \pm 154.0$

Orthogonal form results:

(i) $f^{\rm (cubic)}_{\rm nl} = -155.1 \pm 115.1$
(ii) $f^{\rm (total)}_{\rm nl} = -159.8 \pm 115.1$

[3] The average $\langle q_{ijk} \rangle_{f_{\rm nl}}$ is obtained using 1000 non-Gaussian simulations of the local shape generated by the procedure described in Elsner & Wandelt (2009), and publicly available at http://planck.mpa-garching.mpg.de/cmb/fnl-simulations/.
The best estimates of the local shape presented in Curto et al. (2011b) are $f^{\rm (cubic)}_{\rm nl} = 32.5 \pm 22.5$. Note that in that work, a perturbative approach is considered to simulate the non-Gaussian simulations used to compute $\langle q_{ijk} \rangle_{f_{\rm nl}}$. The different approaches to simulate the non-Gaussianity and the statistical errors due to the finite number of non-Gaussian simulations explain the small differences between the error bars presented here and in that reference.

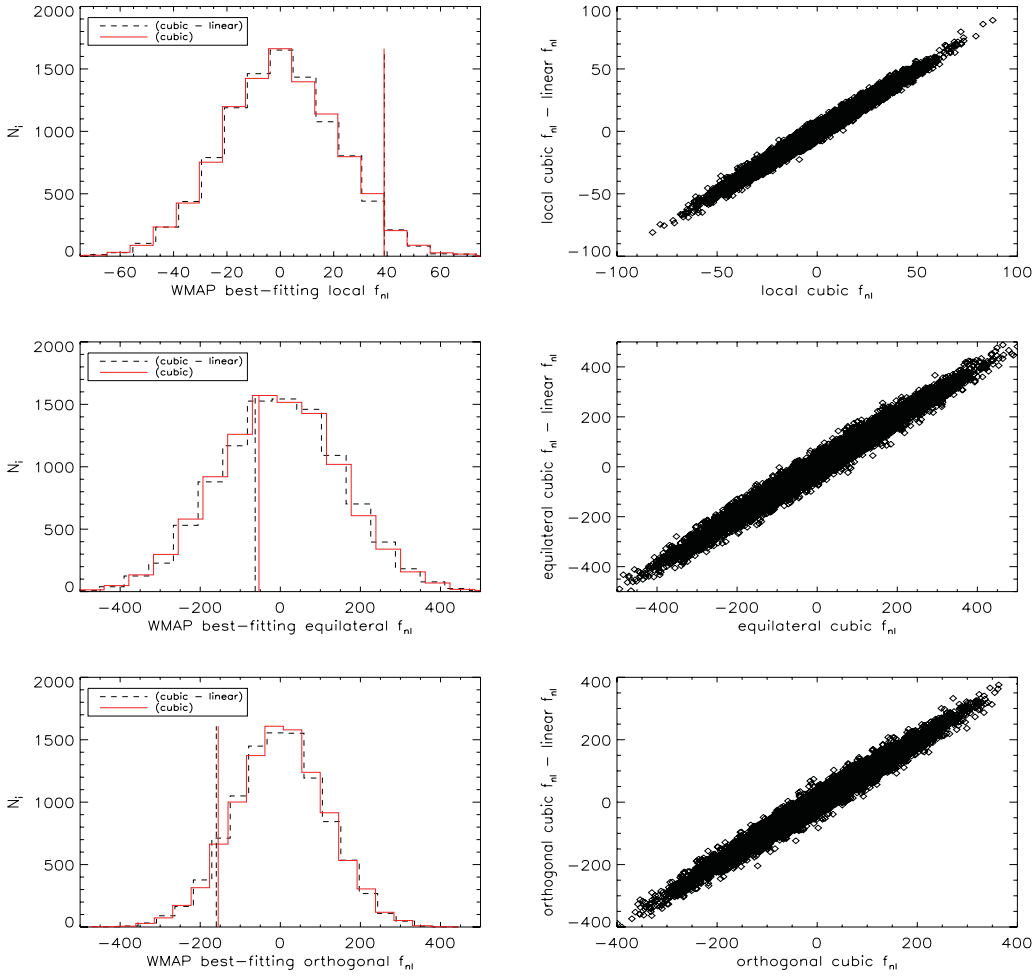

Figure 3. *WMAP* seven-year data best-fitting $f_{\rm nl}$ values using the cubic estimator (equation 11) and the estimator with the linear correction (equation 13) for the local (top), equilateral (middle) and orthogonal (bottom) shapes. In the left-hand panels, the histograms of the best-fitting $f_{\rm nl}$ values with (dashed dark line) and without (solid red line) the linear term correction for each simulation are plotted. The vertical lines correspond to the values obtained with *WMAP* data. The right-hand panels show the corresponding correlation between the same estimates.

Table 1. Constraints on the $f_{\rm nl}$ parameter for the local shape with and without the linear term correction. From left to right, the best-fitting values for the clean and the raw data maps, the mean, dispersion, 16, 84, 2.5 and 97.5 per cent quantiles, respectively, of the $f_{\rm nl}$ distribution obtained with 10 000 Gaussian maps. The Fisher error bar obtained for this shape is $\sigma_{\rm F}(f_{\rm nl}) = 21.6$.

Case	$f_{\rm nl}^{\rm (clean\ data)}$	$f_{\rm nl}^{\rm (raw\ data)}$	$\langle f_{\rm nl}\rangle$	$\sigma(f_{\rm nl})$	X_{16}	X_{84}	$X_{2.5}$	$X_{97.5}$
Cubic	38.9	20.8	0.6	21.6	−21.1	21.9	−42.7	41.8
Linear	−0.1	−0.0	0.0	3.1	−3.1	3.2	−6.1	6.2
Cubic–linear	39.0	20.8	0.7	21.4	−21.0	22.7	−42.6	41.3

Table 2. Constraints on the $f_{\rm nl}$ parameter for the equilateral shape with and without the linear term correction. From left to right, the best-fitting values for the clean and the raw data maps, the mean, dispersion, 16, 84, 2.5 and 97.5 per cent quantiles, respectively, of the $f_{\rm nl}$ distribution obtained with 10 000 Gaussian maps. The Fisher error bar obtained for this shape is $\sigma_{\rm F}(f_{\rm nl}) = 144.5$.

Case	$f_{\rm nl}^{\rm (clean\ data)}$	$f_{\rm nl}^{\rm (raw\ data)}$	$\langle f_{\rm nl}\rangle$	$\sigma(f_{\rm nl})$	X_{16}	X_{84}	$X_{2.5}$	$X_{97.5}$
Cubic	−53.3	28.1	−1.6	154.3	−155.9	151.5	−302.4	302.2
Linear	9.5	13.7	−0.3	23.0	−23.6	22.6	−47.8	46.7
Cubic–linear	−62.8	14.4	−1.3	154.0	−156.4	150.3	−304.5	300.3

Table 3. Constraints on the $f_{\rm nl}$ parameter for the orthogonal shape with and without the linear term correction. From left to right, the best-fitting values for the clean and the raw data maps, the mean, dispersion, 16, 84, 2.5 and 97.5 per cent quantiles, respectively, of the $f_{\rm nl}$ distribution obtained with 10 000 Gaussian maps. The Fisher error bar obtained for this shape is $\sigma_{\rm F}(f_{\rm nl}) = 106.3$.

Case	$f_{\rm nl}^{\rm (clean\ data)}$	$f_{\rm nl}^{\rm (raw\ data)}$	$\langle f_{\rm nl}\rangle$	$\sigma(f_{\rm nl})$	X_{16}	X_{84}	$X_{2.5}$	$X_{97.5}$
Cubic	−155.1	−119.4	0.2	115.1	−113.4	115.2	−230.4	225.6
Linear	4.7	4.8	0.2	18.5	−17.8	18.0	−36.5	36.7
Cubic–linear	−159.8	−124.2	0.0	115.1	−113.2	115.0	−228.4	222.8

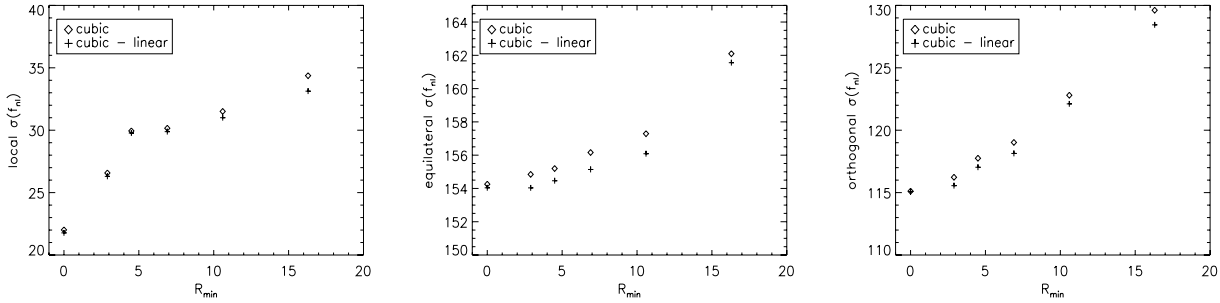

Figure 4. The $f_{\rm nl}$ error bars computed using different $R_{\rm min}$ angular scales for the local (left), equilateral (middle) and orthogonal (right) shapes. The diamonds correspond to $f_{\rm nl}^{\rm cubic}$ and the crosses to $f_{\rm nl}^{\rm total}$.

In order to check that the estimator has already reached optimality with the considered scales for the three shapes, we have computed $\sigma(f_{\rm nl})$ for different subsets of scales (Fig. 4). We compare the $f_{\rm nl}$ error bars for different minimum angular scales $R_{\rm min}$. To find the equivalent multipole ℓ range corresponding to each $R_{\rm min}$ see fig. 5 of Curto et al. (2011a). The three shapes reach minimum variance for $R_{\rm min} = 0$ arcmin.

The error bars of the equilateral and orthogonal shapes are also similar to the values obtained with the direct bispectrum estimator where $\sigma(f_{\rm nl}) = 140$ for the equilateral shape and $\sigma(f_{\rm nl}) = 104$ for the orthogonal shape (Komatsu et al. 2011). The slightly larger values (∼9 per cent) obtained from the dispersion of the $f_{\rm nl}$ distribution corresponding to 10 000 Gaussian simulations, $\sigma(f_{\rm nl}) = 154$ and 115, respectively, are likely due to differences in the perturbative approach used to simulate the non-Gaussian signal of these two shapes (Curto et al. 2011b) or the statistical errors due to the finite number of non-Gaussian simulations.

4 APPLICATION TO *PLANCK* SIMULATIONS

We have computed the linear term correction to the cubic wavelet $f_{\rm nl}$ estimator for the local shape using *Planck* simulations in order to forecast the amplitude of this correction on future *Planck* analyses. We do not consider the two other shapes (equilateral and orthogonal). From the results of the previous sections, we expect the correction for those cases to be even smaller.

For this analysis, we have considered a new set of angular scales that better suits the range of angular multipoles which are cosmic variance dominated ($\ell_{\rm max} \sim 2000$). The list of angular scales is $R_0 = 0$, $R_1 = 1.3$, $R_2 = 2.1$, $R_3 = 3.4$, $R_4 = 5.4$, $R_5 = 8.7$, $R_6 = 13.9$, $R_7 = 22.3$, $R_8 = 35.6$, $R_9 = 57.0$, $R_{10} = 91.2$, $R_{11} = 146.0$, $R_{12} = 233.5$, $R_{13} = 373.6$, $R_{14} = 597.7$ and $R_{15} = 956.3$ arcmin. As a representative mask, we have used the available *WMAP* KQ75 mask (75 per cent of the sky). We have simulated the *Planck* 143 GHz channel using a fiducial CMB power spectrum that best fits *WMAP* 7-year data, $\ell_{\rm max} = 2048$ and a Gaussian beam with FWHM = 7.1 arcmin. The noise has been generated using an anisotropic $N_{\rm hits}$ map computed from the scanning strategy of the *Planck* Sky Model[4] (Delabrouille et al. 2012) and the noise sensitivity per pixel provided in the Planck Bluebook[5] (using an average noise sensitivity for 14 months of $\sigma_{\rm noise} = 2.2\,\mu{\rm K\ K}^{-1}$ in a square pixel whose size is the full width at half-maximum extent of the beam).

The cubic covariance matrix and the linear correlation matrices needed for the $f_{\rm nl}$ estimator in equation (13) have been computed using two independent sets of 10 000 *Planck* Gaussian simulations. The results corresponding to the analysis of an additional set of 1000 Gaussian maps are presented in Fig. 5. Note that for this simulated *Planck* level of anisotropy, $f_{\rm nl}^{\rm (cubic)}$ and $f_{\rm nl}^{\rm (total)}$ are also highly correlated. Finally in Table 4, the properties of the previous histograms are summarized. In particular, we see that using the cubic estimator $\sigma(f_{\rm nl}) = 7.98$, and the linear term contribution reduces this error bar to $\sigma(f_{\rm nl}) = 7.95$ (i.e. a negligible correction lower than 0.4 per cent).

5 CONCLUSIONS

In this paper, we have performed a comprehensive study of the $f_{\rm nl}$ wavelet estimator. We have considered the main statistical assumptions to derive the estimator in terms of the cubic quantities q_i and showed the conditions to reach optimality. We have found that the SMHW wavelet produces an important effective decorrelation of the signal at angular distances above the angular resolution R. This means that the cubic quantities are nearly Gaussian owing to the central limit theorem, and using this property we have found an expression for the likelihood of the $f_{\rm nl}$ parameter in terms of the cubic statistics. We have also included a linear term correction following the Wick polynomials introduced by Donzelli et al. (2012). In particular, we have confirmed that the linear term correction is basically achieved through the mean subtraction that we carry out

[4] http://www.apc.univ-paris7.fr/∼delabrou/PSM/psm.html
[5] The Planck Bluebook is available for download in the web: http://www.rssd.esa.int/index.php?project=Planck

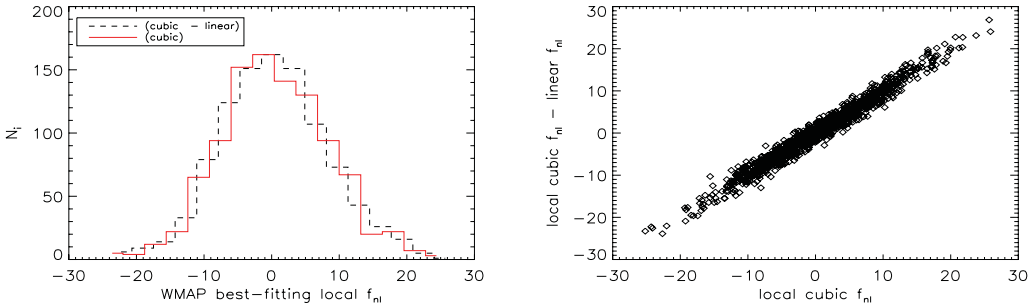

Figure 5. Expected *Planck* 143 GHz best-fitting $f_{\rm nl}$ values using the cubic estimator (equation 11) and the estimator with the linear correction (equation 13) for the local shape. In the right-hand panel, the best-fitting $f_{\rm nl}$ values with and without the linear term correction for each simulation are plotted.

Table 4. Expected constraints on the $f_{\rm nl}$ parameter for the local shape with and without the linear term correction for the 143 GHz *Planck* channel. From left to right, the mean, dispersion, 16, 84, 2.5 and 97.5 per cent quantiles, respectively, of the $f_{\rm nl}$ distribution obtained with 1000 Gaussian maps. The Fisher error bar obtained for this case is $\sigma_{\rm F}(f_{\rm nl}) = 7.5$.

Case	$\langle f_{\rm nl}\rangle$	$\sigma(f_{\rm nl})$	X_{16}	X_{84}	$X_{2.5}$	$X_{97.5}$
Cubic	0.4	7.98	−7.2	8.6	−15.0	17.2
Linear	0.0	1.43	−1.4	1.5	−2.7	2.8
Cubic–linear	0.4	7.95	−7.4	8.2	−15.4	16.7

on the wavelet coefficient maps for each angular scale (Curto et al. 2011a,b). We find that, in this case, the linear term correction only reduces the error bars about 1 per cent for the local case using the *WMAP* data. This correction is even smaller for the equilateral and orthogonal cases (0.2 and 0.1 per cent, respectively). The results presented in this paper are in agreement with the optimal results obtained with the wavelet estimator already published where the mean subtraction was performed (Curto et al. 2009a,b, 2010, 2011a,b). Therefore, we conclude that the contribution of the linear term is negligible (≤ 1 per cent) for the SMHW estimator for the three considered shapes. We have also explored the linear term correction for *Planck* simulations at the 143 GHz channel. Our results indicate that the correction for the local shape is lower than 0.4 per cent considering the expected levels of noise anisotropy for this channel and the *WMAP* KQ75 mask. From the results of *WMAP* data, we expect the correction for the equilateral and orthogonal shapes to be even smaller.

ACKNOWLEDGMENTS

The authors thank Biuse Casaponsa, Simona Donzelli, Michele Liguori, Domenico Marinucci, Sabino Matarrese and Patricio Vielva for useful comments. The authors acknowledge partial financial support from the Spanish Ministerio de Economía y Competitividad project AYA2010-21766-C03-01 and the Consolider Ingenio-2010 Programme project CSD2010-00064. They also acknowledge the computer resources, technical expertise and assistance provided by the Spanish Supercomputing Network (RES) node at Universidad de Cantabria. The authors acknowledge the use of LAMBDA, support for which is provided by the NASA Office of Space Science. The work has also used the software package HEALPIX (Górski et al. 2005). The authors acknowledge the use of the pre-launch *Planck* Sky Model simulation package (Delabrouille et al. 2012).

REFERENCES

Antoine J.-P., Vandergheynst P., 1998, J. Math. Phys., 39, 3987
Babich D., 2005, Phys. Rev. D, 72, 043003
Babich D., Creminelli P., Zaldarriaga M., 2004, J. Cosmol. Astropart. Phys., 8, 9
Bartolo N., Komatsu E., Matarrese S., Riotto A., 2004, Phys. Rep., 402, 103
Bucher M., van Tent B., Carvalho C. S., 2010, MNRAS, 407, 2193
Casaponsa B., Barreiro R. B., Curto A., Martínez-González E., Vielva P., 2011a, MNRAS, 411, 2019
Casaponsa B., Bridges M., Curto A., Barreiro R. B., Hobson M. P., Martínez-González E., 2011b, MNRAS, 416, 457
Cayón L., Martínez-González E., Argüeso F., Banday A. J., Górski K. M., 2003, MNRAS, 339, 1189
Creminelli P., Nicolis A., Senatore L., Tegmark M., Zaldarriaga M., 2006, J. Cosmol. Astropart. Phys., 5, 4
Creminelli P., Senatore L., Zaldarriaga M., 2007, J. Cosmol. Astropart. Phys., 3, 19
Curto A., Martínez-González E., Mukherjee P., Barreiro R. B., Hansen F. K., Liguori M., Matarrese S., 2009a, MNRAS, 393, 615
Curto A., Martínez-González E., Barreiro R. B., 2009b, ApJ, 706, 399
Curto A., Martínez-González E., Barreiro R. B., 2010, in Diego J. M., Goicoechea L. J., González-Serrano J. I., Gorgas J., eds, Highlights of Spanish Astrophysics V. Springer-Verlag, Berlin and Heidelberg, p. 277
Curto A., Martínez-González E., Barreiro R. B., 2011a, MNRAS, 412, 1038
Curto A., Martínez-González E., Barreiro R. B., Hobson M. P., 2011b, MNRAS, 417, 488
Delabrouille J. et al., 2012, preprint (arXiv:1207.3675)
Donzelli S., Hansen F. K., Liguori M., Marinucci D., Matarrese S., 2012, preprint (arXiv:1202.1478)
Donzelli S., Hansen F. K., Liguori M., Marinucci D., Matarrese S., 2012, ApJ, 755, 19
Elsner F., Wandelt B. D., 2009, ApJS, 184, 264
Elsner F., Wandelt B. D., 2010, ApJ, 724, 1262
Elsner F., Wandelt B. D., Schneider M. D., 2010, A&A, 513, A59
Fergusson J., Shellard E. S., 2011, preprint (arXiv:1105.2791)
Fergusson J. R., Liguori M., Shellard E. P. S., 2010a, Phys. Rev. D, 82, 023502
Fergusson J. R., Liguori M., Shellard E. P. S., 2010b, preprint (arXiv:1006.1642)
Górski K. M., Hivon E., Banday A. J., Wandelt B. D., Hansen F. K., Reinecke M., Bartelmann M., 2005, ApJ, 622, 759
Komatsu E., Spergel D. N., 2001, Phys. Rev. D, 63, 063002
Komatsu E., Wandelt B. D., Spergel D. N., Banday A. J., Górski K. M., 2002, ApJ, 566, 19
Komatsu E. et al., 2003, ApJS, 148, 119
Komatsu E., Spergel D. N., Wandelt B. D., 2005, ApJ, 634, 14
Komatsu E. et al., 2009, ApJS, 180, 330
Komatsu E. et al., 2011, ApJS, 192, 18
Liguori M., Sefusatti E., Fergusson J. R., Shellard E. P. S., 2010, Adv. Astron., 2010

Marinucci D. et al., 2008, MNRAS, 383, 539
Martínez-González E., 2008, preprint (arXiv:0805.4157)
Martínez-González E., Gallegos J. E., Argüeso F., Cayón L., Sanz J. L., 2002, MNRAS, 336, 22
McEwen J. D. et al., 2007, J. Fourier Anal. Appl., 13, 495
Pietrobon D., Cabella P., Balbi A., de Gasperis G., Vittorio N., 2009, MNRAS, 396, 1682
Rudjord Ø., Hansen F. K., Lan X., Liguori M., Marinucci D., Matarrese S., 2009, ApJ, 701, 369
Sanz J. L., Herranz D., López-Caniego M., Argüeso F., 2006, preprint (arXiv:astro-ph/0609351)
Senatore L., Smith K. M., Zaldarriaga M., 2010, J. Cosmol. Astropart. Phys., 1, 28
Smidt J., Amblard A., Byrnes C. T., Cooray A., Heavens A., Munshi D., 2010, Phys. Rev. D, 81, 123007
Smith K. M., Senatore L., Zaldarriaga M., 2009, J. Cosmol. Astropart. Phys., 9, 6
Spergel D. N. et al., 2007, ApJS, 170, 377
Vielva P., 2007, in Van De Ville D., Goyal V. K., Papadakis M., eds, Proc. SPIE Vol. 6701, Wavelets XII. SPIE, Bellingham, p. 670119
Vielva P., Martínez-González E., Tucci M., 2006, MNRAS, 365, 891
Yadav A. P. S., Wandelt B. D., 2008, Phys. Rev. Lett., 100, 181301
Yadav A. P. S., Wandelt B. D., 2010, Adv. Astron., 2010
Yu H.-R., Harnois-Déraps J., Zhang T.-J., Pen U.-L., 2012, MNRAS, 421, 832
Zhang T.-J., Yu H.-R., Harnois-Déraps J., MacDonald I., Pen U.-L., 2011, ApJ, 728, 35

This paper has been typeset from a TEX/LATEX file prepared by the author.